Journal of Power Sources 240 (2013) 252–257

Contents lists available at SciVerse ScienceDirect

Journal of Power Sources

journal homepage: www.elsevier.com/locate/jpowsour

Short communication

New insights into the mechanism of pseudocapacitance deterioration in electrodeposited MnO_2 under negative potentials

Suzana Sopčić [a], Robert Peter [b], Mladen Petravić [b], Zoran Mandić [a,*]

[a] Faculty of Chemical Engineering and Technology, University of Zagreb, Marulićev trg 19, HR-10000 Zagreb, Croatia
[b] Department of Physics and Center for Micro and Nano Sciences and Technologies, University of Rijeka, Rijeka 51000, Croatia

HIGHLIGHTS

- Capacitance deterioration mechanism of MnO_2 investigated by CV, EQCM, XPS and SEM.
- The irreversible transformation of MnO_2 is taking place at negative potentials.
- The transformation is accompanied by the uptake of large quantities of water.
- The charging/discharging mechanism changes reflecting the appearance of Mn_2O_3.

ARTICLE INFO

Article history:
Received 11 January 2013
Received in revised form
14 March 2013
Accepted 3 April 2013
Available online 10 April 2013

Keywords:
MnO_2
Supercapacitors
Capacitance deterioration
EQCM

ABSTRACT

The mechanism of deterioration of the capacitive response of electrodeposited MnO_2 under reducing potentials has been studied by combined electrochemical and quartz crystal microbalance, XPS and SEM techniques. Cycling of the electrode towards cathodic potentials of −0.3 V *vs.* Ag/AgCl leads to irreversible reduction resulting in low valence manganese oxide, most probably Mn_2O_3. The reduction is accompanied by phase transformation with the uptake of considerable amounts of water into the layer. The capacitive behaviour of the MnO_2 electrode fades with prolonged cycling with the concomitant change of charging/discharging mechanism.

1. Introduction

The charge storage reaction of manganese oxides is actively investigated due to their importance in such applications as active electrode materials in batteries and supercapacitors. Most authors agree that the mechanism of the redox reaction involves simultaneous electron and proton insertion/deinsertion, which can be described by Equation (1).

$$MnO_2 + H^+ + e^- \rightarrow MnOOH \quad (1)$$

If the reaction takes place in moderate or highly alkaline media, alkali metal cations could participate in the reaction instead of protons and generally the reactions can be written as in Equation (2).

$$Mn(IV)O_2 + xe^- + xM^+ \rightarrow M_xMn(III)_xMn(IV)_{1-x}O_2 \quad (2)$$

This reaction represents a solid state homogenous reaction, giving rise to the rectangular current profile frequently observed during linear voltage sweep experiments with manganese oxide electrodes. Even though this reaction looks simple, consisting of only a few elementary processes, its detailed mechanism is still largely unknown. In fact, it seems that the overall charging/discharging reaction consists of several distinct, highly overlapping processes. Some authors have identified as many as nine processes in a relatively narrow potential range around 0.7 V [1]. Their results demonstrated that proton diffusion through the MnO_2 material is a rate limiting process [2,3].

In order to better understand factors that control this reaction, much research effort has been devoted to revealing the peculiarities of this system and to developing electrode materials with improved charge storage capabilities. Even though the theoretical gravimetric capacitance of this material exceeds 1300 F g^{-1}, such values are rarely observed in practice due to the limiting diffusion rate of protons and/or sodium ions towards the deeper layers of oxide. The slow diffusion results in low utilization of the bulk redox

* Corresponding author. Tel.: +385 1 4597164; fax: +385 1 3733640.
E-mail address: zmandic@fkit.hr (Z. Mandić).

0378-7753/$ – see front matter © 2013 Elsevier B.V. All rights reserved.
http://dx.doi.org/10.1016/j.jpowsour.2013.04.008

centres in MnO_2, resulting in practical gravimetric capacitances far below the theoretical value, *i.e.*, usually around 200 F g^{-1}. To overcome the inherent sluggishness of the proton diffusion and increase utilization of the bulk material, attempts have been made to prepare MnO_2 electrodes in the form of thin films [4] or to prepare various MnO_2/carbon nanostructures [5,6].

Another limitation of manganese oxide electrodes in supercapacitor applications is their usable voltage range. The anodic cut-off voltage is determined by the oxygen evolution reaction which commences at potentials around 0.8 V *vs*. an Ag/AgCl reference electrode [7]. Potentials below 0.2 V *vs*. Ag/AgCl induce undesirable capacitance deterioration, becoming more pronounced at more negative potentials. The capacitance deterioration mechanism is still not completely understood. Most authors agree it is caused by irreversible structural changes in the solid state. However, some authors attribute this change to the dissolution–redeposition mechanism of Mn(III) species at negative potentials [8,9], while others ascribe it to an irreversible charge transfer process leading to an electrochemically inactive material [10–12].

In this paper we report on new findings regarding the capacitance fading mechanism of anodically deposited MnO_2 (EMD) at a gold electrode. Using combined electrochemical and quartz crystal microbalance (EQCM) techniques, we demonstrate that the irreversible reduction taking place at negative potentials is accompanied by considerable uptake of water into the MnO_2 layer, followed by structural transformations exhibiting a different mechanism for the charging/discharging reaction over a wide potential range.

EQCM has already been used several times for the investigation of the deposition process of manganese oxide [13–18] as well as its reaction mechanism [14]. In the latter case the measurements were only performed over a limited potential range, and showed monotonic mass changes during voltammetric cycling, *i.e.*, mass decrease during oxidation and mass gain during reduction, confirming the redox mechanism of manganese oxide represented by Equation (1).

2. Materials and methods

2.1. MnO_2 electrode preparation

MnO_2 layers were electrodeposited on a gold covered quartz crystal electrode from a 0.25 M $MnSO_4 \cdot 4H_2O$ solution (Alfa Aesar) at a constant potential of 0.9 V *vs.* Ag/AgCl (3 M KCl) during 150 s. Platinum sheet served as a counter electrode. The geometric area of the working electrode was 0.2 cm^2. The Sauerbrey equation was used to estimate the deposited MnO_2 mass from quartz crystal frequency changes, with an integral sensitivity $C_f = 1.96 \times 10^8$ Hz cm^2 g^{-1}. XRD analysis revealed completely amorphous structure of deposited MnO_2 layer. The thickness of deposited MnO_2 layer was estimated from deposited mass taking into account MnO_2 density of $\rho = 5.026$ g cm^{-3}. Its value was approximately 7 μm.

2.2. Electrochemical measurements

Both cyclic voltammetric and chronoamperometric measurements were carried out using a EG&G M263A potentiostat in a three-electrode experimental setup with electrodeposited MnO_2 on a 9 MHz AT-cut quartz crystal (Seiko QCA 917) as a working electrode, Ag/AgCl (3 M KCl) as a reference and Pt-sheet as a counter electrode. All measurements were done in 0.5 M Na_2SO_4 supporting electrolyte. Cyclic voltammetric measurements were performed by repetitive cycling over the potential range, either from 0.2 V to 0.6 V or from −0.3 V to 0.6 V with a scan rate of 50 mV s^{-1}. Chronoamperometry was performed by potential steps, either from 0.2 to 0.6 V or from −0.3 to 0.6 V and *vice versa*. Molar mass calculations of the exchanged ionic species were done as described previously [19].

2.3. XPS analysis

XPS spectra were recorded under UHV conditions (typical pressure in the 10^{-7} Pa range) in a SPECS system with a Phoibos MCD 100

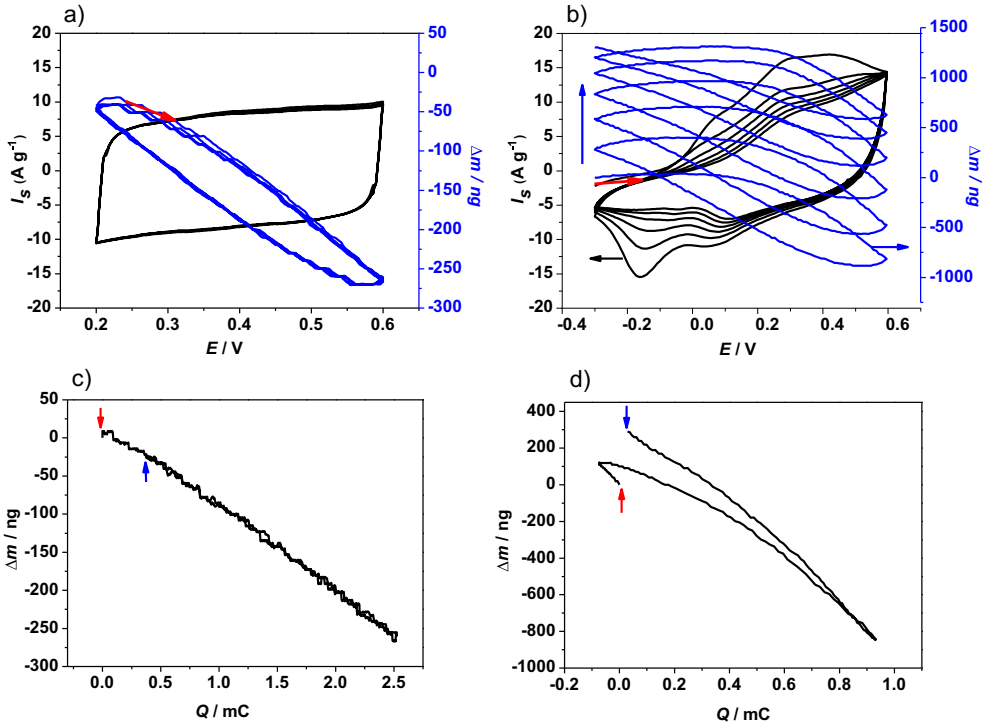

Fig. 1. Combined cyclic voltammetry and EQCM investigations of electrodeposited MnO_2 in the potential ranges (a) 0.2 to 0.6 V, (b) −0.3 to 0.6 V and corresponding mass–charge plots constructed from (c) the first cycle in the range 0.2 to 0.6 V, (d) the first cycle in the range −0.3 to 0.6 V. Scan rate = 50 mV s^{-1}.

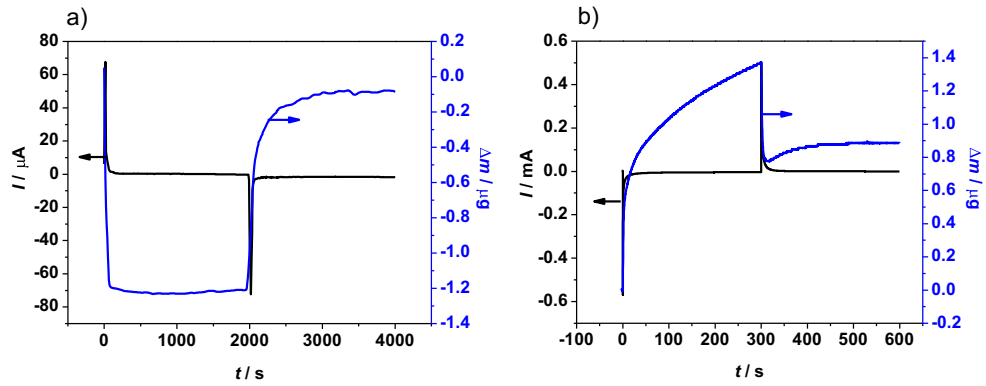

Fig. 2. Current responses and simultaneous mass changes in MnO_2 electrode after potential steps from (a) 0.2 to 0.6 V and back to 0.2 V, (b) 0.6 to −0.3 V and back to 0.2 V.

electron analyser and monochromatized Al K_α X-rays of 1486.74 eV. For the pass energy of 10 eV used in the present study, the total energy resolution was better than 0.8 eV. The photoemission spectra were simulated with several sets of mixed Gaussian–Lorentzian functions with Shirley background subtraction.

3. Results and discussion

Fig. 1a and b shows the simultaneous voltammetric response of a MnO_2 electrode and its mass change during five consecutive cycles from 0.2 to 0.6 V and from −0.3 to 0.6 V, respectively. The flat current profile and rectangular shape of the cyclic voltammograms recorded when the electrode was cycled from the cathodic potential of 0.2 V confirmed the suitability of the MnO_2 electrode in supercapacitor applications. The response was stable and reversible during prolonged cycling and no appreciable capacitance drop was observed. Gravimetric capacitance of 160 F g^{-1} was obtained using Sauerbrey equation taking into account mass calculated from quartz crystal frequency difference before and after MnO_2 deposition. This valued is in accordance with the usually observed specific capacitances obtained for the MnO_2 electrodes with thicknesses in micrometer range [18]. Simultaneous EQCM results (blue curve in the web version) show mass decrease during oxidation and mass gain during reduction. These results are in accordance with the reaction mechanism described by Equation (1).

From the EQCM results and cyclic voltammograms it is possible to construct mass change *vs.* charge plots, given in Fig. 1c for the first voltammetric cycle from Fig. 1a. Such a plot is useful since it reveals several important features of the MnO_2 oxidation/reduction mechanism. First of all, if charge represents the MnO_2 oxidation state, then the linearity of the mass–charge dependence unambiguously demonstrates the uniformity of the reaction mechanism throughout the investigated potential range. Since the slope is constant, a single ionic species is exchanged between the oxide layer and solution during electrochemical reaction. The molecular mass, *M*r, of the exchanged ionic species can be calculated from the slope [20], which for the results given in Fig. 1c amounts to about 70 Da. This value is higher than would be expected from Equation (1), where either a proton (*A*r = 1) or Na^+ (*A*r = 23) is exchanged. The most plausible explanation is that protons leave and enter the MnO_2 as a species coordinated with a variable amount of water.

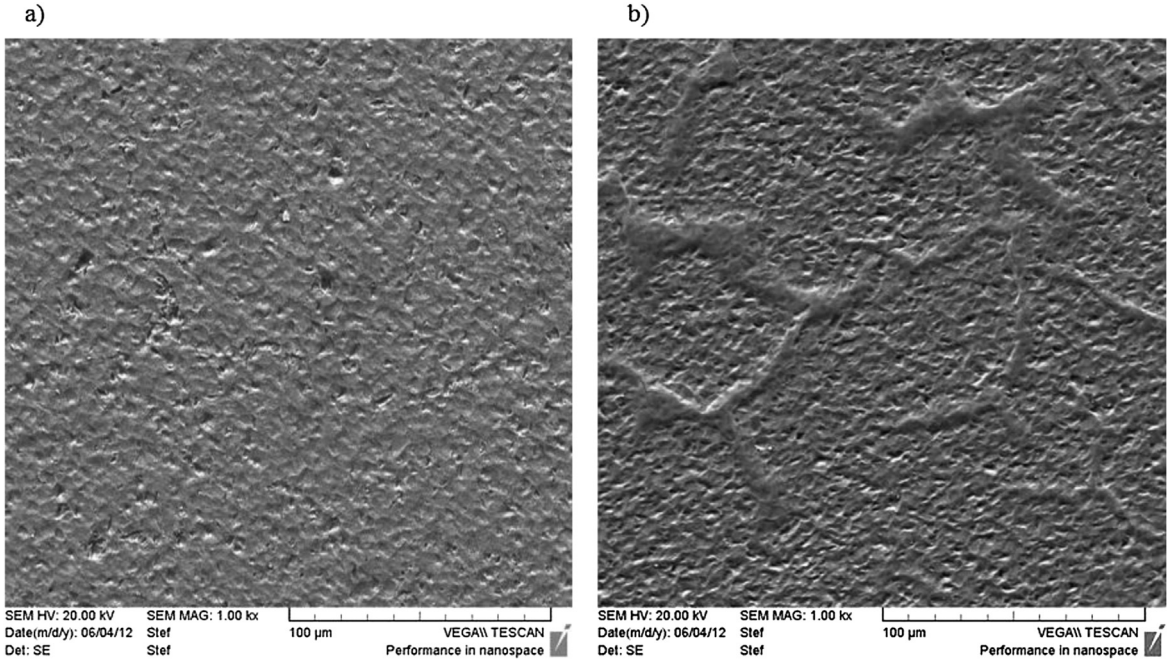

Fig. 3. SEM micrographs of the surface of (a) freshly prepared MnO_2 electrode and (b) MnO_2 electrode after 30 continuous voltammetric cycles from −0.3 to 0.6 V.

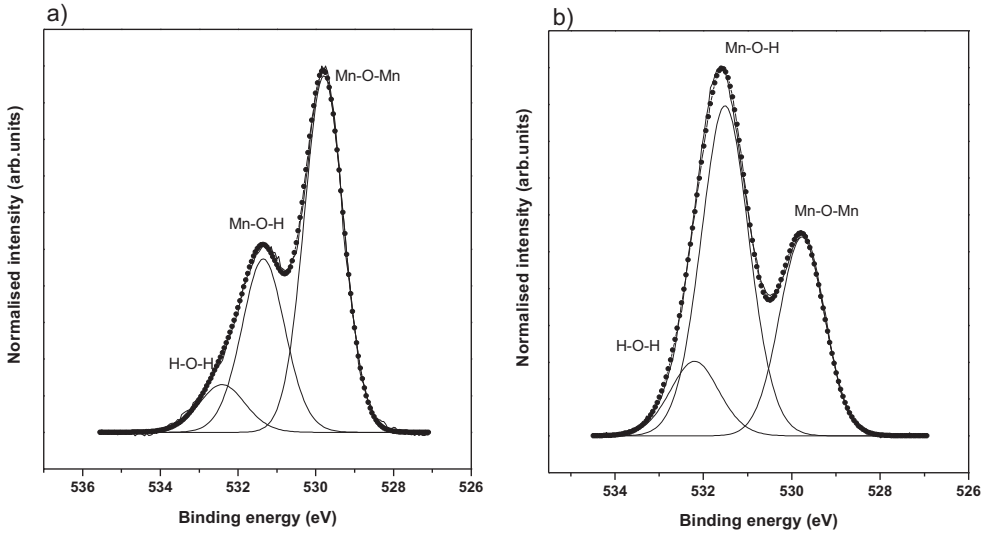

Fig. 4. O1s photoemission spectra of (a) freshly prepared MnO_2 and (b) MnO_2 reduced at −0.3 V during 30 s.

The second important property of the MnO_2 charging/discharging reaction to be concluded from the mass–charge plot in Fig. 1c is the chemical reversibility of the MnO_2 oxidation/reduction reaction in the potential range 0.2–0.6 V. The mass–charge plot shows no hysteresis, and the mass of the electrode precisely overlaps at each oxidation state regardless of the direction of potential change.

Finally, although the mass of the electrode precisely corresponds to the oxidation state of the oxide, its oxidation state does not reach the oxidation state it had at the beginning of the voltammetric cycle. This result reveals the thermodynamic irreversibility of the electrochemical reaction, *i.e.*, the sluggishness of the reduction comparing to the rate of the oxidation reaction. This is probably due to slow proton diffusion into the deeper layers of the bulk MnO_2, as already confirmed in several papers [2].

The electrochemical behaviour of the MnO_2 electrode when cycled from a cathodic potential of −0.3 V exhibited completely different characteristics. Two reduction current peaks were observed at potentials more negative than 0.2 V and the capacitive response of the electrode deteriorated rapidly with cycling (Fig. 1b). Simultaneous electrode mass monitoring revealed the usual electrochemical behaviour of MnO_2 in the 0.2–0.6 V potential range. No appreciable mass change was observed in the anodic part of the cyclic voltammogram between −0.3 and 0.2 V. However, the mass of the electrode increased continuously over the whole cathodic potential sweep. The most peculiar observation is that the total electrode mass increased with each consecutive voltammetric cycle. These two experimental facts clearly indicate that electrochemical reduction of MnO_2 at cathodic potentials more negative than 0.2 V is accompanied by an irreversible chemical reaction resulting in solid state transformation of the oxide. The potential dissolution of low-valence manganese species could not be detected either because it did not take place or it was not significant reaction in the overall net change. Due to the concomitant loss in capacitive response, the solid state transformation is obviously unfavourable from the standpoint of the application of manganese oxide in supercapacitor applications.

The mass–charge plot constructed from the first voltammogram in Fig. 1b is shown in Fig. 1d. In contrast to the mass–charge plot obtained from the results in the limited potential range starting from 0.2 V, here a significant deviation between the cathodic and anodic branches can be noticed. This indicates that the process occurring at cathodic potentials is both chemically and thermodynamically irreversible.

In order to investigate the nature of the accompanying chemical reaction and reveal the corresponding changes in the oxide layer,

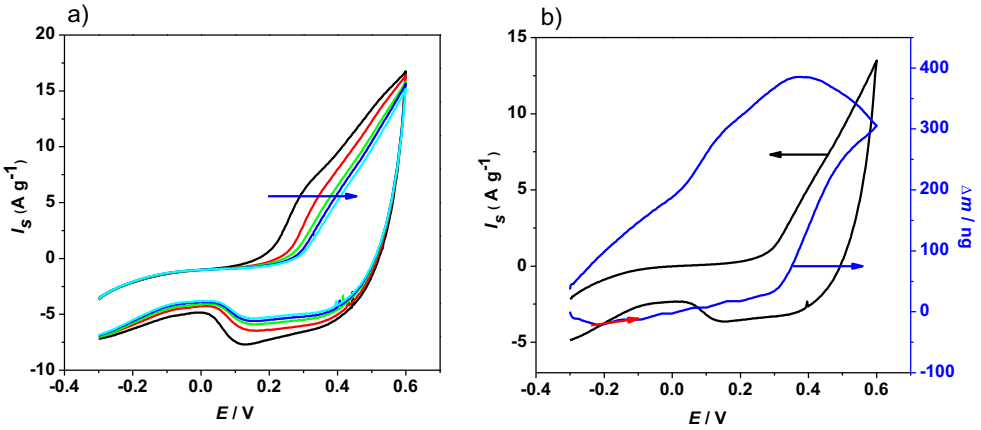

Fig. 5. (a) The evolution of cyclic voltammograms after 200 successive cycles and (b) simultaneous cyclic voltammogram and corresponding mass change from the selected cycle in (a). Scan rate = 50 mV s^{-1}.

chronoamperometric measurements (Fig. 2), SEM micrographs (Fig. 3) and XPS spectra (Fig. 4) were taken.

Potential jumps between potentials belonging to the reversible behaviour of MnO_2 (Fig. 2a) resulted in fast current and mass change responses. After the current induced by each potential jump dropped to zero, the mass of the electrode assumed a constant and stable value. For the reduction part of the transient current, the time required to reach the constant mass of the electrode is somewhat longer, confirming the earlier observation of the sluggishness of the reduction reaction compared to its oxidation counterpart.

When transient currents were recorded by jumping the potential from the reversible region (0.6 V) to the irreversible region (−0.3 V), the mass of the electrode did not reach the stable value even after the current fell to zero (Fig. 2b). Instead, a continuous, almost linear mass increase was registered. The mass gain with time is obviously not connected with the charge transfer anymore, but rather to the uptake of a significant amount of water taking place at the surface of the reduced form of manganese oxide. Substitution of Mn^{4+} by Mn^{3+} leads to lattice expansion and an increase in the volume of the unit cell, as predicted from radii data on Mn cations and as observed experimentally [21], creating enough space for water uptake. There are at least two types of water that could be associated with the reduced manganese structure, one being structural water in the form of OH^- ions replacing O^{2-} in the lattice as charge compensation and the other being interstitial water. SEM micrographs of MnO_2 electrode taken after prolonged cycling (Fig. 3b) show partial and irregular swelling of the surface comparing to the freshly prepared MnO_2 electrode (Fig. 3a). The overall chemical transformation is irreversible, leading to the electrochemically inactive layer being unsuitable for applications of the material in supercapacitors.

The surfaces of MnO_2 samples were also analysed by XPS. Fig. 4 shows O1s photoemission spectra for freshly prepared MnO_2 (Fig. 4a) and MnO_2 reduced at −0.3 V during 30 s (Fig. 4b). Both spectra were deconvoluted into three contributions (solid lines in Fig. 4) with binding energies of 529.8 eV, 531.4 eV and 532.3 eV, respectively. The first two lines are attributed to oxygen atoms bound to manganese atoms in higher and lower oxidation states represented by Mn–O–Mn or Mn–O–H bond configurations, respectively [4,6,15]. The latter peak is assigned to oxygen from water molecules (H–O–H bonds). The XPS analysis indicates the quite different content of Mn–O–Mn and Mn–O–H bonds in these samples. The Mn–O–Mn contribution is dominant in freshly prepared MnO_2, while the Mn–O–H content is larger in the reduced sample of MnO_2. In addition, curve-fitting shows a larger content of water in the electrochemically treated sample. The XPS results confirm that the second reaction, which has led to an overall mass increase, is an irreversible reduction of MnO_2 accompanied by a hydration reaction which takes place after successive cycling of MnO_2 towards negative potentials.

As a consequence of the structural transformations of the manganese oxide, not only is the overall capacitance of the electrode lost but the complete mechanism of the charging/discharging reaction also changes. As seen in Fig. 5a, the flat current profile usually registered in the potential region 0.2 to 0.6 V gradually transforms into a shape characteristic of an electrochemical reaction in a layer possessing two distinct phases of reactants and products. At the same time, the registered EQCM profiles undergo smooth transition from the behaviour displayed in Fig. 1b to completely opposite behaviour, *i.e.*, the mass of the electrode increases during oxidation and decreases during reduction (Fig. 5b). The transition takes place over 200 cycles and corresponding mass–charge curves for selected cycles are shown in Fig. 6.

Taking into account that the irreversible reactions at negative potentials lead to low valence manganese oxides such as Mn_2O_3,

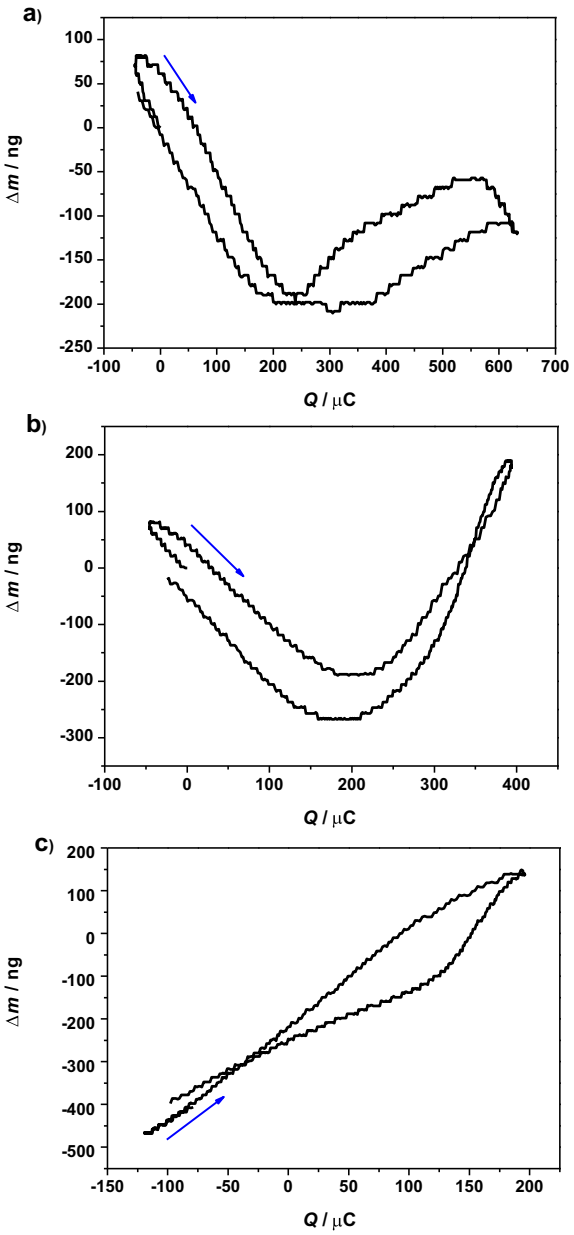

Fig. 6. Mass–charge plots of the continuously cycled MnO_2 electrode in the potential range −0.3 to 0.6 V; (a) 100th, (b) 150th and (c) 200th voltammetric cycle.

the electrochemical charging/discharging reaction can now be written as:

$$Mn_2O_3 + H_2O \rightarrow 2MnO_2 + 2e^- + 2H^+ \quad (3)$$

Suggested charging/discharging mechanism complies with the direction of mass changes during oxidation and reduction reactions of MnO_2 and explains reasonably well the overall electrochemical behaviour of MnO_2 electrode as well as structural transformations taking place at sufficiently negative cathodic potentials.

4. Conclusions

Electrodeposited manganese oxide undergoes irreversible reduction at potentials more negative than 0 V *vs.* an Ag/AgCl reference electrode. This reduction leads to low-valence

manganese oxide, most probably Mn_2O_3. As demonstrated by EQCM and XPS measurements, the reduction is accompanied by the uptake of water. As a result, the charging/discharging mechanism changes from pseudocapacitive behaviour to a process resembling a solid state electrochemical reaction, where both reactants and products exist in two distinct, separate phases.

Acknowledgement

Financial support by Ministry of Science, Education and Sports of Republic of Croatia (project 125-1252973-2576) is gratefully acknowledged. We thank Stjepan Kožuh for taking SEM images and György Inzelt and Marijana Kraljić Roković for fruitful discussions.

References

[1] G.J. Browning, S.W. Donne, J. Appl. Electrochem. 35 (2005) 437–443.
[2] G.J. Browning, S.W. Donne, J. Appl. Electrochem. 35 (2005) 871–878.
[3] X. Xi, L. Hong, C. Zhenhai, J. Electrochem. Soc. 136 (1989) 266.
[4] M. Toupin, T. Brousse, D. Belanger, Chem. Mater. 16 (2004) 3184.
[5] K.W. Nam, C.W. Lee, X.Q. Yang, B.W. Cho, W.S. Yoon, K.B. Kim, J. Power Sources 188 (2009) 323–331.
[6] E. Raymundo-Pinero, V. Khomenko, E. Frackowiak, F. Beguin, J. Electrochem. Soc. 152 (2005) A229.
[7] F. Ataherian, N.L. Wu, J. Electrochem. Soc. 158 (2011) A422–A427.
[8] W. Wei, X. Cui, W. Chen, D.G. Ivey, J. Power Sources 186 (2009) 543–550.
[9] S.C. Pang, M.A. Anderson, T.W. Chapman, J. Electrochem. Soc. 147 (2000) 444.
[10] Y.C. Hsieh, K.T. Lee, Y.P. Lin, N.L. Wu, S.W. Donne, J. Power Sources 177 (2008) 660–664.
[11] F. Ataherian, K.T. Lee, N.L. Wu, Electrochim. Acta 55 (2010) 7429–7435.
[12] K.W. Nam, M.G. Kim, K.B. Kim, J. Phys. Chem. C 111 (2007) 749.
[13] G. Moses Jacob, I. Zhitomirsky, Appl. Surf. Sci. 254 (2008) 6671–6676.
[14] S. Devaraj, N. Munichandraiah, Electrochem. Solid State Lett. 12 (2009) F21–F25.
[15] M.P. Owen, G.A. Lawrance, S.W. Donne, Electrochim. Acta 52 (2007) 4630–4639.
[16] P.K. Nayak, S. Devaraj, N. Munichandraiah, Electrochem. Solid State Lett. 13 (2010) F29–F32.
[17] Y.H. Chu, C.C. Hu, H.K. Chang, Electrochim. Acta 61 (2012) 124–131.
[18] S.L. Kuo, N.L. Wu, J. Electrochem. Soc. 153 (2006) A1317–A1324.
[19] S. Sopčić, Z. Mandić, G. Inzlet, M. Kraljić Roković, E. Meštrovi&cacute, J. Power Sources 196 (2011) 4849–4858.
[20] S. Sopčić, M. Kraljić Roković, Z. Mandić, A. Róka, G. Inzelt, Electrochim. Acta 56 (2011) 3543–3548.
[21] P. Ruetschi, J. Electrochem. Soc. 131 (1984) 2737–2744.